# MAGNETOTELLURIC INVESTIGATION OF THE CAUSATIVE FAULT OF THE 2016 MW 5.8 PAWNEE, OKLAHOMA EARTHQUAKE

By

DAVID JAMES BECKENDORFF

Bachelor of Science in Geology

Texas A&M University

College Station, Texas

2016

Submitted to the Faculty of the
Graduate College of the
Oklahoma State University
in partial fulfillment of
the requirements for
the Degree of
MASTER OF SCIENCE
May, 2018

MAGNETOTELLURIC INVESTIGATION OF THE

CAUSATIVE FAULT OF THE 2016 MW 5.8

PAWNEE, OKLAHOMA EARTHQUAKE

Thesis Approved:

Dr. Estella Atekwana

Thesis Adviser

Dr. Mohamed Abdelsalam

Dr. Ahmed Ismail

ACKNOWLEDGEMENTS

I would like to acknowledge first my advisor Dr. Estella Atekwana, without whom I would have not been at this point. I consider myself lucky to have been mentored by such a hardworking and inspiring person who never stopped pushing me and believing in me. I would also like to thank my parents and brothers who stood behind me the entire time and helped me believe in myself.

Also, I cannot thank enough the group of graduate students who helped me do the manual labor required in the field and never complained. Throughout this project, Micah Mayle, Victor Nyalugwe, Janot Ngalamo, Folarin Kolawole, Nathan Campbell, Brandon Chase, Chloe Gustafson and Daniel Blatter have helped answer any and all questions and I cannot thank them enough for all of their help. The whole BPSoG was always friendly and helping since I came into the program and just were accepting since the beginning.

I would also like to thank Dr. Kerry Key of Columbia University and Dr. Rob Evans of Woods Hole Oceanographic Institution (WHOI) for both supplying the magnetotelluric (MT) equipment and teaching the BPSoG students how to use them. Without them this project could not have happened.

Lastly, I just want to thank my advisor Dr. Estella Atekwana again and also the rest of my committee, Dr. Mohamed Abdelsalam and Dr. Ahmed Ismail who were helpful to me during this process. As well as the National Science Foundation Grant # 1664474 which funded this project.

Name: TYPE NAME

Date of Degree: MAY, 2016

Title of Study: MAGETOTELLURIC INVESTIGATION OF THE CAUSATIVE FAULT OF THE 2016 MW 5.8 PAWNEE, OKLAHOMA EARTHQUAKE

Major Field: GEOLOGY

Abstract:

On September 1, 2016 a Mw 5.8 earthquake struck the Pawnee area of north central Oklahoma. The rupture occurred in a region of complex fault interactions at 4 -6 km depth, along a previously unmapped fault called the Sooner Lake Fault.Seismic studies suggest this fault is a near vertical (70-90 degree dip), left lateral strike-slip fault. Despite broad agreement between activities related to hydrocarbon production and induced seismicity, we do not fully understand the linkages between injection, subsurface fluid migration, and pressure build-up along faults. Not every injection well is associated with seismicity, and not every fault in a newly seismic region is reactivated by oil and gas production activities. This study deployed magnetotelluric (MT) instruments to better understand the relationship between induced seismicity and waste water injection. The MT data was acquired across 18 MT stations along a profile line perpendicular to the geoelectric strike of the Sooner Lake Fault. This data was imported into the WingLink software with which an inversion was carried out to image the rupture zone. The resulting MT cross-section clearly imaged an upper layer of conductive sediments and a conductive wedge associated with the rupture zone of the Sooner Lake Fault within the resistive basement. The ~4 km wide base of this conductive wedge is found at ~12 km depth and tappers out upward to a depth of ~6 km. The hypocenters of the earthquakes coincide with the tip of this conductive wedge.

TABLE OF CONTENTS

LIST OF FIGURES

Figure Page

Figure Page

# CHAPTER I

## INTRODUCTION

The September 3, 2016 Mw 5.8 Pawnee earthquake in north central Oklahoma is the largest earthquake in the Mid – Continent region of the United States that might have been induced by waste water injection. It was one of many seismic events in central Oklahoma (Figure 1 A and B) that are considered to have been triggered by waste water injection related to hydrocarbon production (Yeck et al. 2016). Prior to 2009, there was approximately only one M ≥3.0 earthquake per year. Since then, magnitude 3.0 or greater have increased up to 300 times (Figure 2) (McNamara et al. 2015; Langenbruch and Zoback, 2016) with notable events including the 2011 Mw 5.7 Prague earthquake, 2016 Mw 5.1 Fairview earthquake, and the 2016 Mw Cushing earthquake which was preceded by two Mw 4.0 earthquakes in 2015 (Figure 1). The year of 2009 not only saw a major increase in seismic activity, but also a rise in the volume of waste water injection as shown in Figure 2 comparing the rise in earthquakes with the rise in waste water injection and their relationship. Most of the injected waste water is targeting the highly permeable Arbuckle Formation due to its low pressure conditions (Langenbruch and Zoback, 2016).

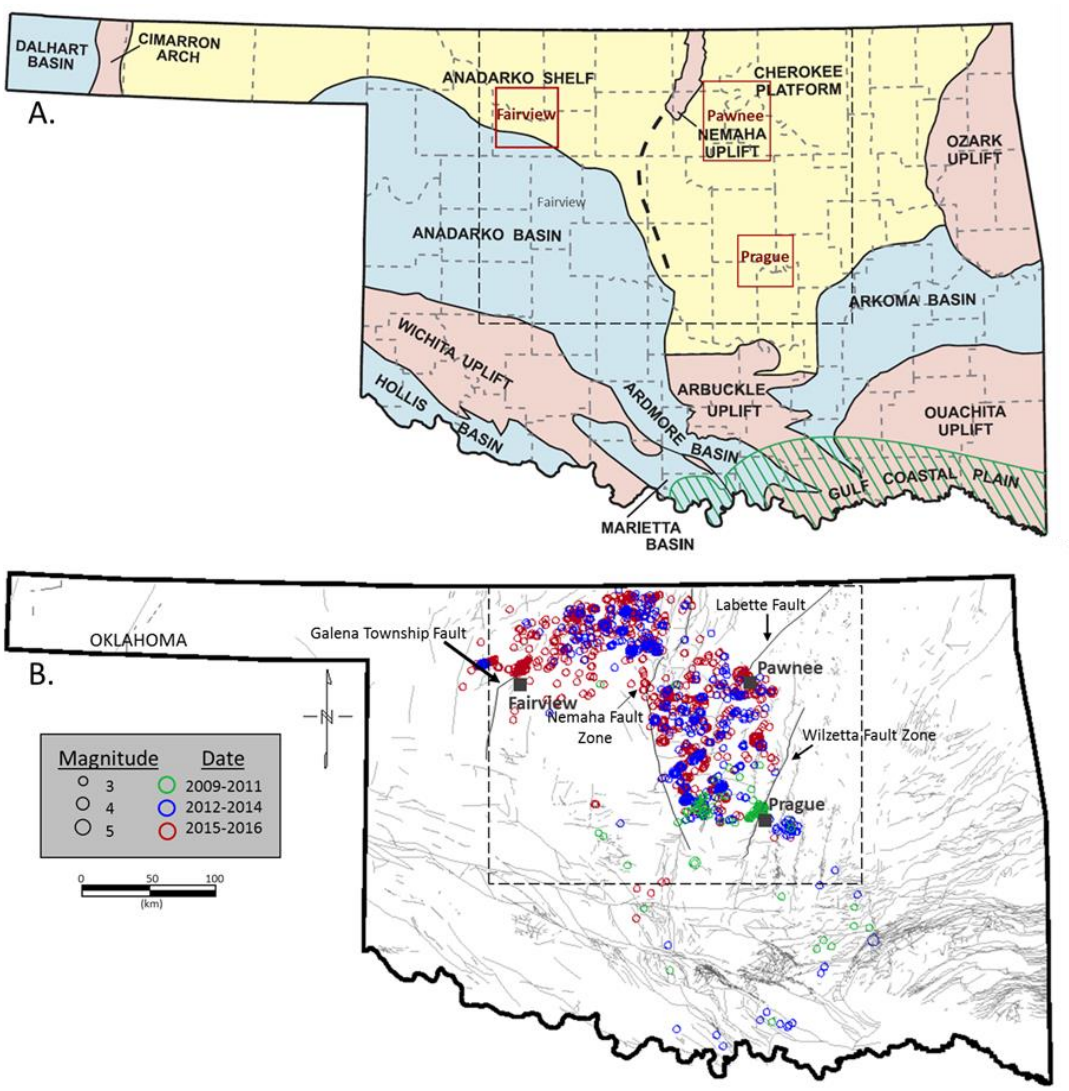


Figure 1. A) Generalized tectonic provinces of Oklahoma modified from Northcutt and Campbell (1995). Locations of three study major earthquake areas shown by red boxes. B) Map showing Oklahoma Geological Survey epicenter locations of earthquakes Mw ≥3.0 occurring from 2009 – 2016. Grey lines represent fault locations as indicated by the Oklahoma Geological Survey fault layer. Not the locations of major faults and fault zones: the Nemaha Fault Zone, the Wilzetta Fault Zone, the Labette Fault, and the Galena Township Fault (Adapted from Harding, 2017).

Keranen et al. (2013) first highlighted the spatiotemporal correlations between the 2009 Prague Mw 5.6 earthquake and the waste water injections (within neighboring wells) and suggested that the injection related to pore fluid pressure increases induced the earthquakes. Since the Keranen et al. (2013) study, multiple geophysical studies have suggested that injected waste water within subsurface formation can migrate into Precambrian basement faults and increase pore fluid pressure, which in turn reduces the frictional resistance to slipping, leading to seismic rupture of these faults (Keranen et al. 2014; Langenbruch and Zoback, 2016; Nolte et al. 2017 and references therein).

An experiment conducted in the 1960's was one of the earliest studies to document the correlation between pumping water into the subsurface and the triggering of seismicity (Healy et al. 1968). Since then, numerous studies have documented the association between fluid and gas injection and induced seismicity. More recent studies have suggested that fluid injection can trigger earthquakes as far as 10-20 km from the injection well (Keranen et al. 2013). In fact, a study by Yeck et al. (2016) suggested that the epicenter of the Mw 5.1 2016 Fairview earthquake is located more than 12 km away from the high-rate injection wells, confirming that the effect of waste water injection can be wide spread. More recently, in the Mid – Continent of the United States, Nolte et al., (2017) used time-lapse shear wave (S-wave) anisotropy analysis to provide direct evidence linking earthquake occurrence to pore pressure increase. The Nolte et al. (2017) study which began in 2010, analyzed S-wave splitting data to demonstrate the increase of pore pressure in the subsurface. Subsequently, using spatiotemporal analysis of the location of the waste water injection wells and the occurrence of earthquakes, they were able to directly link the increased seismicity with increased pore pressure. Further, Nolte et al. (2017) conducted an anisotropy analysis and found that the fast S-wave direction flipped $90^{o}$ from being in line with the maximum horizontal stress to now being in line with the minimum horizontal stress. Nolte et al. (2017) further suggests that this has been caused by an increase in pore fluid pressure that is

high enough to hold saturated fractures open that would normally be closed. This phenomenon of S-wave flipping was first observed by Angerer et al. (2002) from $CO_2$ injection wells, which caused an increase in pore fluid pressure in a fractured reservoir located in the Vacuum Field in the Permian Basin in New Mexico (Angerer et al. 2002).

The use of this space-time distribution of the earthquakes in Oklahoma infers that this marked increase in seismicity is caused by anthropogenic activities, mainly due to wastewater injection. Figure 2 (Chen et al. 2017) shows the noticeable increase in seismicity with the increase of the number of wastewater injection wells and the increase in the volume of water injected. During 2015, a restriction by the state was placed on wastewater injection after the 2014 Prague earthquake. As shown in Figure 2, the frequency of earthquakes started declining shortly after 2015, correlating to the decline of wastewater injection.

.

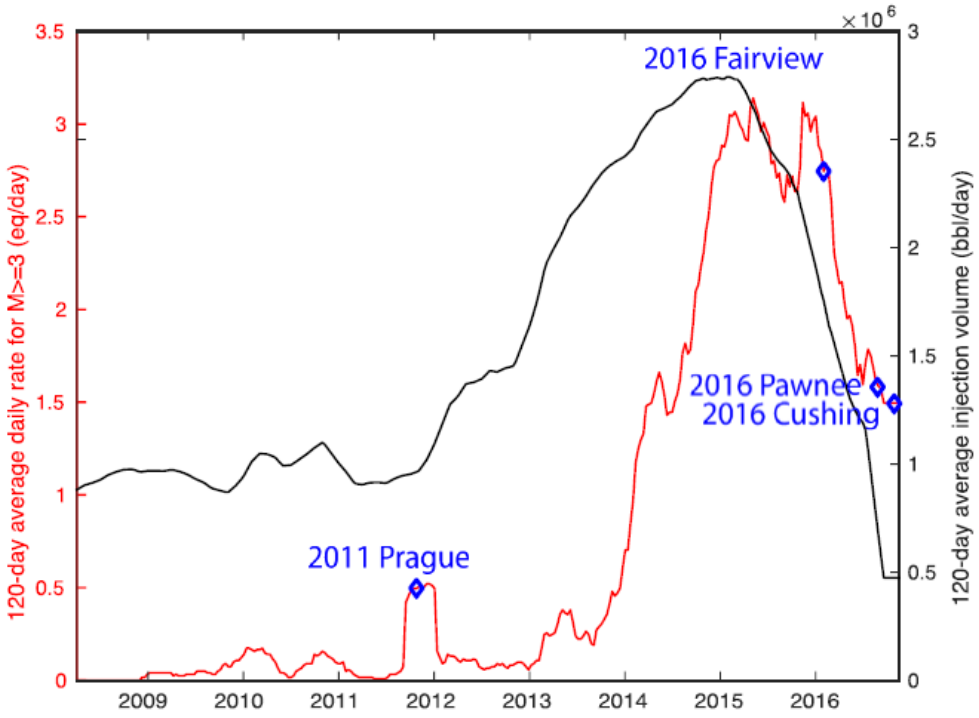


Figure 2. The correlation between the frequency of Mw >3.0 earthquake occurrence and waste water injection volume between 2009 and 2016 (After Chen et al. 2017).

Despite broad agreement between the spatial correlations between activities related to hydrocarbon production and induced seismicity, we do not fully understand the linkages between the injection activities, subsurface fluid migration, and pressure build-up along faults that are prone to rupture, hence causing earthquakes. Not every waste water injection well can be spatially correlated with seismic activity, and not every fault found within a newly seismic region is considered to be reactivated by hydrocarbon production activities For example, McNamara et al. (2015) conducted an extensive study in the Cushing area of Oklahoma area where two moderate earthquakes (Mw 4.0 and Mw 4.3) occurred in October 2014. Through spatial and kinematic analysis, they mapped a complex system of reactivated, previously unknown conjugate sets of strike-slip structures within the Wilzetta-Whitetail fault zone. After analyzing the spatial distribution of seismic events and regional moment tensor focal mechanisms, McNamara et al. (2015) mapped the Cushing Fault, a left-lateral strike-slip fault that runs conjugate to the main branch of the Wilzetta-Whitetail fault zone.

To predict and mitigate future hazard in Oklahoma, characterization of the faults that are most likely to be reactivated is important. Several types of investigations have been undertaken to investigate the faults that are found within the Precambrian basement. Harding (2017) used aeromagnetic data to investigate seismic zones in Oklahoma including Fairview, Prague, Cushing, and Pawnee earthquakes. The Harding (2017) study suggested that, besides the low resolution of the aeromagnetic data, because the Precambrian basement is dominantly made-up of granitic rock, there is little to no contrast in the magnetic anomalies. For the Pawnee area, it was found that most of the seismic events occur at the intersection of the Labette Fault and Sooner Lake Fault. Further, Harding (2017) hypothesized that most earthquakes in the area have occurred due to the bi-material makeup and brittleness of the basement rock contained in the intersection of the Labette Fault and SLF. Harding (2017) identified a positive magnetic anomaly in the Fairview region and interpreted it as a NE-SW trending lithological contact between different

Precambrian basement rocks. Harding (2017) observed that the spatial distribution of aftershock are aligned with the boundary, and proposed that the Galena Township Fault follows this lithological contact. Another magnetic anomaly was observed over the Prague region, where a small series of faults conjugate to the main branch of the Wilzetta Fault were observed. One thing to note from the Harding (2017) study was the anomaly shown in the Fairview study area which suggested that the earthquake ruptured along the edge of a magnetic high or basement intrusion and the anomaly in the Pawnee study area showed a NW-SE trending linear feature. Harding (2017) results inferred that most of these reactivated faults are confined to basement depths of 1.5 km – 2.5 km. Shah and Keller (2017) mapped where most earthquakes occurred in the Precambrian crystalline basement in Oklahoma using a combination of gravity and magnetic data and drill hole data. They observed a regional correlation between the occurrence of seismicity and the location of waste water injection wells. Interestingly, there were some local areas that showed higher amounts of seismic activity than other areas. They found that lithological variation has an influence on the occurrence of the induced seismicity. Shah and Keller (2017) observed that areas of fractured intrusive and metamorphic rock within the Precambrian basement have higher concentration of earthquakes than areas covered by thick sedimentary and extrusive volcanic rocks.

The results from the Shah and Keller (2017) study show how seismicity is not solely controlled by injection rates of waste water but is also highly influenced by subsurface geologic features. The increased occurrence of seismicity in the intrusive and metamorphic rocks could be caused by the high intensity of fractures providing pathways for the injected waste water to percolate through the rock mass and cause pore fluid pressure changes (Shah and Keller, (2017).

Other studies used passive seismic data to map the spatial distribution and kinematics of fault and concluded that the majority of these reactivated faults within which earthquakes occurred are strike-slip with earthquake focal depths between 2 km and 8 km (e.g., Fielding et al.

2017). Although passive seismic techniques are best for locating earthquakes and deduce the kinematics of the associated ruptured faults, these techniques are unable to predict the location of faults that are prone to future rupture due to migration of fluids, hence causing earthquakes. Magnetotelluric (MT) studies, however have been extensively used in the past to image fault zones and detect the presence of fluids, because fluids-hosting faults have high electrical conductivity relative to their host rocks. For example, Becken et al. (2008) inverted MT data from 66 sites along a profile line across the San Andreas Fault to create a two-dimensional (2D) electrical resistivity models to map the relative distribution of fluids within this fault system. The Becken et al. (2008) MT models showed a high conductive zone, inferred to be fluids present in the fault zones aligned along a NE portion of the San Andreas Fault where seismic activities are known to occur in the past. Therefore, in this study, the MT technique is used to image the Sooner Lake Fault zone in the area of the 2016 Mw 5.8 Pawnee earthquake

# CHAPTER II

# STUDY AREA

## *2.1 The Basement of Oklahoma*

The exposed part of the Precambrian crystalline basement of Oklahoma is represented by the Southern Granite Rhyolite Province, and the igneous and metamorphic rock predominantly date to the Precambrian and Cambrian ages (Denison, 1966). Most of what is known about the Oklahoma Precambrian crystalline basement at the sub-surface comes from the hydrocarbon exploration wells that penetrated down to the basement as well as geophysical data. For example, Denison (1966, 1981) utilized wells that were drilled to basement in connection with the analysis of regional gravity and magnetic data to subdivide the basement into four major rock units dating back to the Mesoproterozoic era (1285 ∓18 Ma). These units shown in Figure 3 are as follows from oldest to youngest: the Washington Volcanic Group, the Spavinaw Granite Group, the Osage Microgranite, and the Central Oklahoma Group.

The Washington Volcanic Group is important to this study because it is found at the sub-surface around the Pawnee area; the subject of this study. Denison (1966, 1981,1984) described the Washington Volcanic Group as a sequence of thick flows and tuffs consisting primarily of rhyolites and a band of metarhyolites due to regional metamorphism. The Spavinaw Granite is an

intrusive, felsic granite composed of micrographic granite porphyry. This is thought to be one complex that was due to multiple injection beneath the volcanic cover. The Osage microgranite is interpreted as a thin sill composed of porphyritic rocks. This unit lies beneath the center of Osage County, Oklahoma. The last and youngest unit is the Central Oklahoma Granite Group. This is thought to have formed from multiple intrusions of a composite batholith because of its large area and contact metamorphism of rhyolites to metarhyolites (Denison, 1966, 1981, 1984).

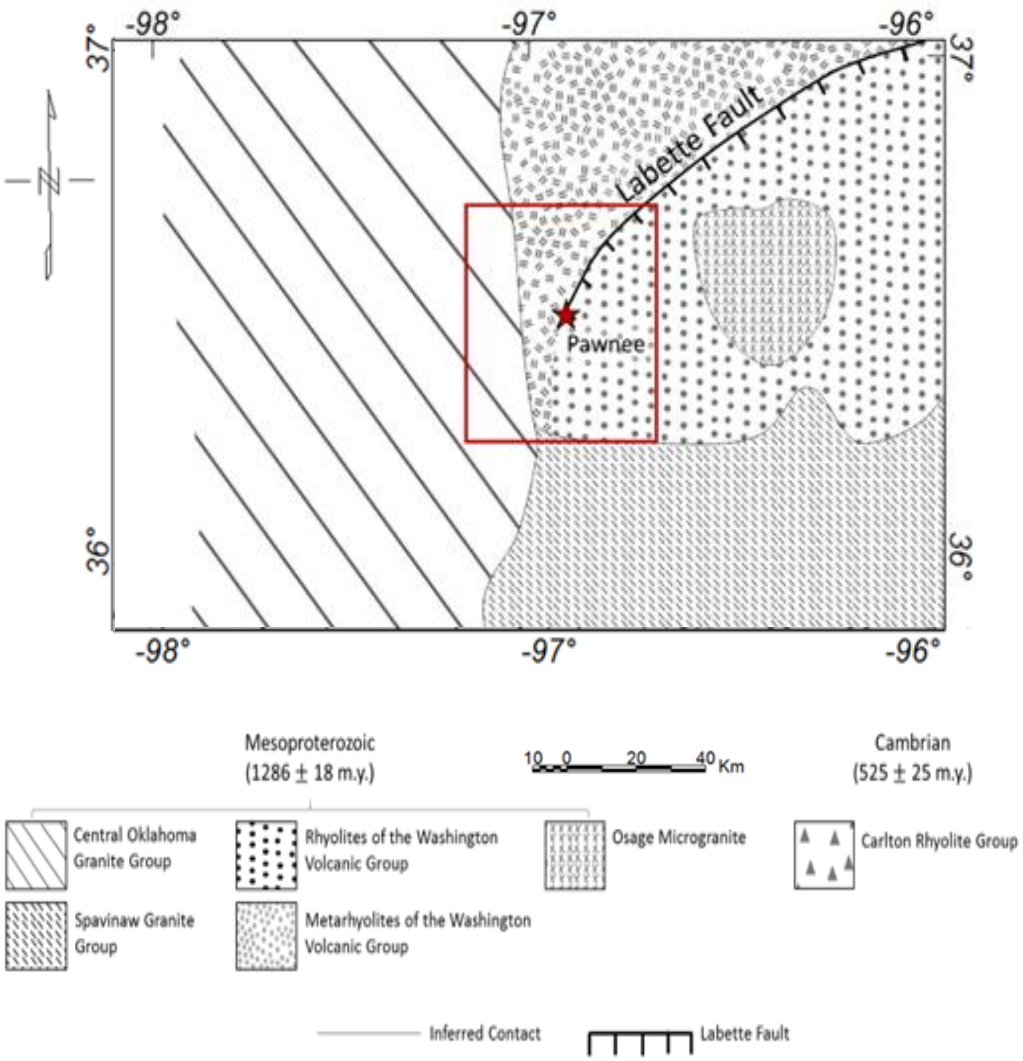


Figure 3. Geological basement map of the Precambrian crystalline basement of Pawnee area modified from Denison (1981; 1984). The red star is the location of the Mw 5.8 earthquake.

### *2.2 Geologic Setting*

The State of Oklahoma is located within the Mid - Continent region of the United States in which repeated tectonic events have resulted in six major episodes and basins development. According to Northcutt and Campbell (1995), since the boundaries are structural, these provinces can be considered a generalized tectonics map (Figure 1A) and are the result of tectonics and the resulting sedimentation. Oklahoma consists of a series of complex fault systems, which include the NW-SE trending Meers Fault, the N-S trending Nemaha Fault, the NNE-SSW trending Wilzetta Fault, the N-S Watchorn Fault, and the NNE-SSW trending Labette Fault (Figure 1B). The study area in Pawnee, Oklahoma where the 2016 Mw 5.8 earthquake occurred is located on the Cherokee Platform and the shelf of the Arkoma Basin.

The 2016 Mw 5.8 earthquake occurred at the newly identified Sooner Lake Fault, which had not been previously mapped (Figure 4). This reactivated fault is located between the two major fault systems of the N-S Watchorn Fault and the NNE-SSW Labette Fault. These two major faults are part of the Nemaha Fault Zone, which originated during the Middle Ordovician (466 Ma) (Mcbee, 2003). The Labette Fault, which originated during the Mesoproterozoic (1000 Ma) is a basement rooted, compensating fault that goes through part of the study area (Denison, 1981; Harding, 2017). The Sooner Lake Fault (SLF) is delineated by the spatial distribution of the aftershocks and focal plan mechanism solution $107^{o}$ striking and $90^{o}$ dipping left-lateral strike-slip (Pennington and Chen, 2017). Interestingly, the Watchorn Fault was not reactivated at all and the Labette Fault was only partially reactivated on its northern segment during the Pawnee earthquake

The study area is surrounded by multiple wastewater injection wells in all directions, one within 10 km, with the majority of the injection wells injecting waste water into the under-

pressured Arbuckle Group (Figure 5) consisting of limestone and dolomites from the Ordovician – Cambrian times (Grandin et al., 2017). However, the direct connection between the injected wastewater in Pawnee area and the seismic rupture at depth in the basement is yet to be established. In order to establish this link, MT technique was applied to image the Sooner Lake Fault Zone in the area of seismic rupture.

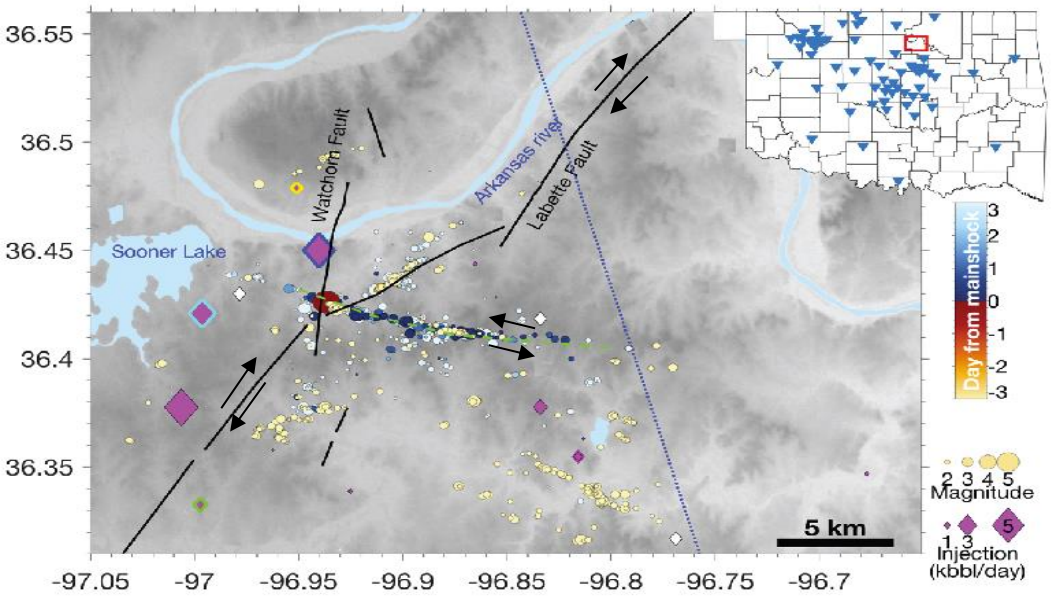


Figure 4. Distribution of earthquake epicenters, waste water injection wells, and the trace of known faults in the Pawnee area with the faults slip shown. The blue dashed line represents the geologic cross – section shown in Figure 5 (After Chen et al. 2017).

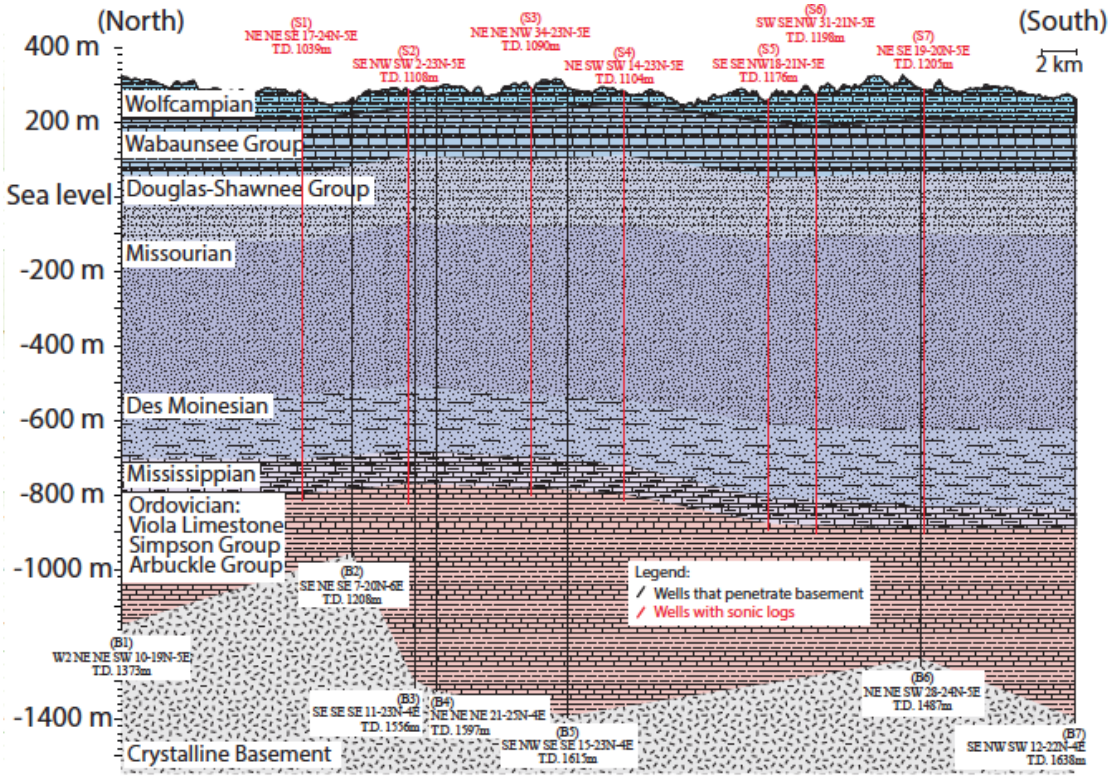


Figure 5. NNW-SSE stratigraphic cross-section showing major stratigraphic units beneath Pawnee region (After Chen et al. 2017). Note that the depth to the Precambrian crystalline basement is between 1100 and 1500 m. Location of profile is shown on Figure 4.

### *2.3 Site History*

The Pawnee area contains a complex fault system consisting of the Watchorn Fault, the Labette Fault, and the Sonner Lake Fault (Figure 4). The latter two of the three faults are interconnected. Pennington and Chen (2017) studied the roles that static coulomb stresses play due to foreshocks, mainshock, and aftershocks. Focusing on the Pawnee earthquake, Pennington and Chen (2017) considered three Mw ≥ 3.0 that occurred prior to the September 1 quake and one Mw ≥ 3.0 aftershock that occurred less than five days after the mainshock. After analyzing the three foreshocks, the results showed an increase in the coulomb stress by 0.69 – 1.98 bars at the hypocenter of the mainshock. Figure 6 shows the seismic profile lines of Chen et al. (2017) seismic events along the Sooner Lake Fault, seismogenic depths, and the foreshocks, mainshock, and aftershock events. From this, the main seismogenic depths can be seen between 4-6 km with an average magnitude between 2-4 km, which when referring back to Figure 5, is well within the crystalline basement.

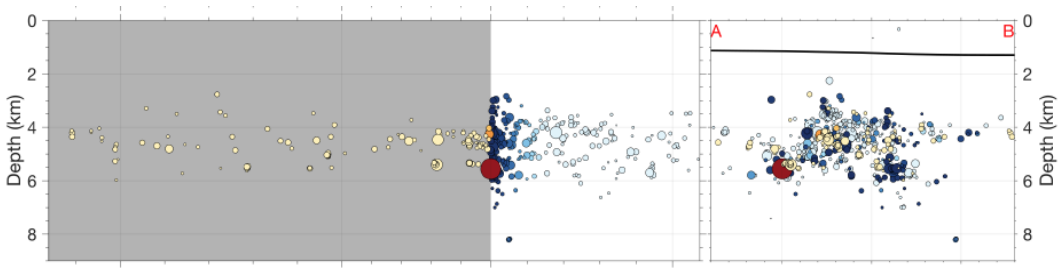


Figure 6. Seismogenic depths along the profile line with most seismicity occurring between 4-6 km. The colored circles are the relocated earthquakes with the same color scheme as Figure 4 (Adapted from Chen et al. 2017).

# CHAPTER III

# METHODOLOGY

## *3.1 Principles of the Magnetotelluric (MT) Method*

The Magnetotelluric (MT) method is a natural-source technique, meaning that it measures the orthogonal time-varying electric and magnetic fields. From these two measurements, the conductivity of the sub-surface is obtained (Cagniard, 1953). The natural-sources can be divided into two categories: low frequency and high frequency. Low frequency sources include solar winds, while high frequency sources can be due to lightning storms, which transmit their energy into the ionosphere. In the MT technique, electromagnetic waves transmit their energy through the ionosphere and head vertically into earth due to the high contrast of the earth – air boundary (Vozoff, 1991). These waves then propagate through the sub-surface generating the eddy currents within the sub-surface conductors that then generate the important secondary currents, which is what is measured at the surface. The conductivity of the layers these waves are traveling through will affect both the amplitude and phase of the secondary electric field (Bedrosian, 2007). Magnetotelluric techniques measure the secondary magnetic fields and then transforms them to the frequency domain, which is broken down to the linear vectors of the electric field (E), and the magnetic field (H) shown below:

Equation 1: $\begin{bmatrix} E_x \\ E_y \end{bmatrix} \begin{bmatrix} Z_{xx} & Z_{xy} \\ Z_{yx} & Z_{yy} \end{bmatrix} \begin{bmatrix} H_x \\ H_y \end{bmatrix}$

To get the apparent resistivity and phase values, the Z vector, called the magnetotelluric impedance tensor, is used in Cagniard's formula (Cagniard, 1953).

Equation 2: $\rho_{xy} = \frac{1}{\omega \mu_0} \left| Z_{xy} \right|^2, \varphi_{xy} = \tan^{-1}\left[ Z_{xy}(\omega) \right]$

Equation 3: $\rho_{yx} = \frac{1}{\omega \mu_0} \left| Z_{xy} \right|^2, \varphi_{yx} = \tan^{-1}\left[ Z_{yx}(\omega) \right]$

Where $\omega$ is the angular frequency and $\mu_0$ is the permeability of free space (Cagniard, 1953).

The end result of the measurements of magnetotellurics needs to be in terms of Transverse Electric (TE), which is denoted by the X direction and the Transverse Magnetic (TM) which is denoted by the Y direction. To calculate these two values, the observed impedance tensor must be found. Due to the data sets dealing in the 2D, Equation 4 will contain two zeroes at a diagonal and two non-zeroes in the other diagonal. One of these two non-zero values will be the X($Z_{xy}$) which represents the current flowing along the geological strike and the other non-zero value, Y($X_{yx}$) is the current flowing across the strike. These two terms combined make up the sounding curves shown in Equation 5 and 6.

Equation 4: $Z_{obs} = R Z_{2D} R^T = R \begin{bmatrix} 0 & Z_{xy} \\ Z_{yx} & 0 \end{bmatrix} R^T$

Equation 5: $E_x(\theta) = Z_{xy} H_y(\theta)$

Equation 6: $E_y(\theta) = Z_{yx} H_x(\theta)$

When dealing with the propagating electromagnetic waves moving through the layers of Earth, the skin effect must be taken into account. The Skin effect is the decrease or decay of the

electric signal as it moves deeper and deeper and through the different mediums until it can no longer be detected or is 1/e of its original value measured at the surface. With this knowledge, the depth of investigation can be estimated. The resistivity of the layers (ρ) and the frequency (ω) are two controlling factors of the skin depth (δ).

$$\text{Equation 7 : } \delta = \sqrt{\frac{2\rho}{\mu\omega}} \approx 500\sqrt{\frac{\rho}{f}}\,\text{meters}$$

(μ is magnetic permeability)

From this equation, it can be gathered that the lower the frequency, or higher resistivity will give greater depths of penetration into the sub-surface (Cagniard, 1953).

### *3.2 Field Acquisition*

In this study, two different types of magnetotellurics (MT) instruments were used: the long period LEMIs with a period of 20-100 seconds, and the short period, high frequency broadband Zens ranging from $10^{-3}$ – $10^{3}$ seconds. The MT data was acquired over the months of October and November 2016, a month after the Pawnee earthquake occurred.

The long term LEMI instruments were left out for three weeks at a time, measuring a wideband, low frequency MT response using induction coil magnetometers. The low frequency of the LEMIs allows for deeper penetration of the subsurface down to tens of km. The Zen instruments are a broadband, higher frequency system (16 Hz) which gives a better resolution but can only penetrate a maximum of 10 km. These systems were left out to continuously collect data over-night and were able to be moved to a new location each day.

For this survey, 4 LEMI and 14 Zen stations were placed along the line, which was aligned to the geoelectric strike of the Sooner Lake Fault (SLF) and the survey is shown in Figure

7. The LEMI stations were placed approximately 1 km apart from each other while the Zen stations were placed together two at a time with a 500 m spacing approximately for each set. Both systems had a similar layout with 50 m dipole lines going in the N-S, and E-W directions with electrodes at each end (A schematic diagram is shown in Figure 8). The main difference in the systems parts were the magnetometers. The LEMI system had one magnetometer, while the Zen system had three, one for each of the X, Y, and Z components. Using the combination of the two systems along with the spacing allowed us to get both the depth of penetration and the high resolution to image the subsurface of Pawnee and the Sooner Lake Fault.

B.

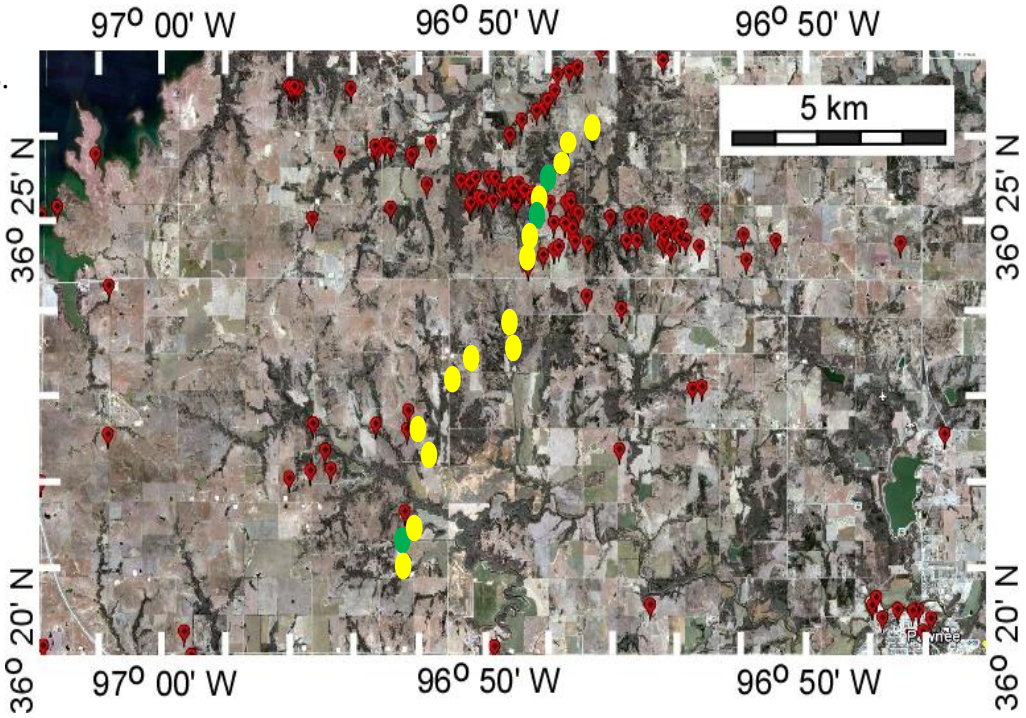


Figure 7. Natural color 3-2-1 red-green-blue (RGB) color combination Landsat Thematic Mapper ™ image of the Pawnee area showing the location of the magnetotelluric (MT) stations (Zens marked by yellow filled circles and LEMIs marked by green filled circles) used to collect data in this study. The image is obtained from Google Earth Pro.

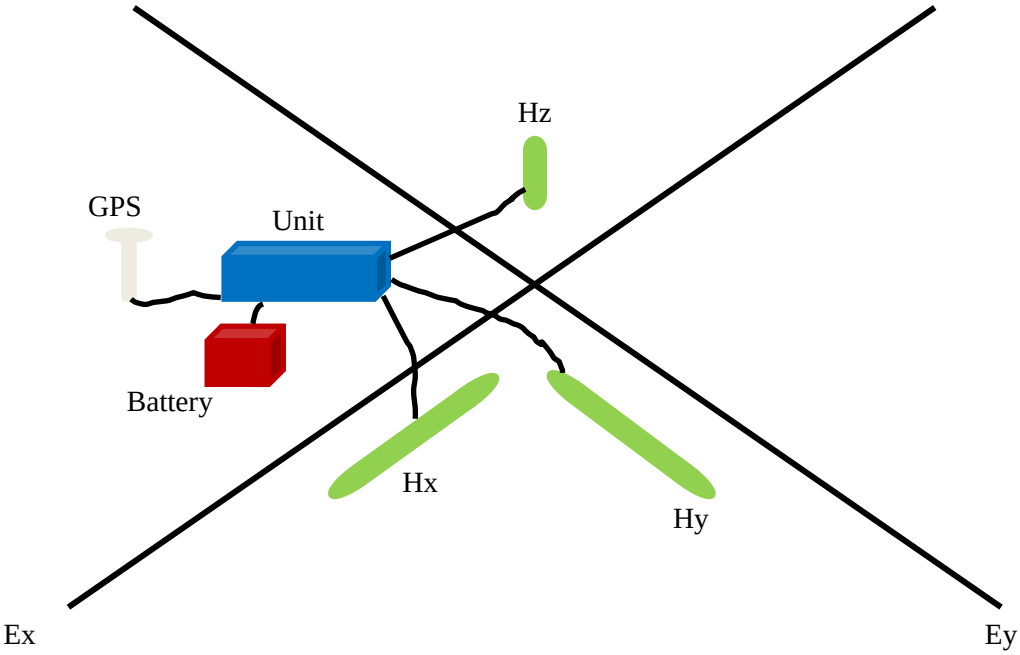


Figure 8. A schematic diagram of the field layout for the MT system (Credit to A Jones Dublin EM short course).

### *3.3 MT Data Processing*

The processing of the MT data was a two part process. For the Zen data, the data were processed using a robust multiple station method that uses data from two or more receivers to robustly separate the MT plane wave signal from local noise. To do this the MT time series are chopped up into many short time segments, are Fourier transformed to the frequency domain and then the MT impedance tensor is solved for (Egbert, 1997). Once that was completed, all the data was loaded into WingLink, the Transvers Electric (TE) and Transverse Magnetic (TM) lines for each station were closely examined graphically and any points that were noisy, did not line up, or had a very high error were hidden and not used in the inversion process. This process must be done with extreme care because if too much data is taken out, there will not be enough to extrapolate and run the inversion program with a high enough resolution and low error.

Once the TE and TM lines have been cleaned, a 2D inversion can be ran. A grid was created along the profile line made up of 99 rows and 141 columns. The inversion solved for the smoothest model, using a standard grid Laplacian operator. The minimum frequency used for the TE and TM data was 0.0001 Hz.

To help analyze the fit of the 2D inversion model, pseudo-sections can be created to compare the observed apparent resistivity against the calculated resistivity. Pseudo-sections read the apparent resistivity values for each station against the measured parameter values for each station along the MT profile line, then interpolates them to show any changes in the subsurface. Two separate pseudo-sections were created, one with the raw data from the field and one using the software 2D inversion model created (Figure 9 and 10). Figure 9 shows the pseudo-section created for the TE and TM lines using the raw data from the field, 3 possible layers are shown in both the transverse electric and transverse magnetic sections and both pseudo-sections appear to be similar showing a good fit. Moving to Figure 10, the pseudo-section using the 2D inversion

data, as a first step of the data inversion, the software plots the observed (field data) and calculates an initial model based on the observed data. When comparing the observed against the calculated, 3 layers are seen, the TE and TM profiles match up well with the TM matching almost perfectly and the TE just having a slight discrepancy in the deepest most resistive part. However, these pseudo-sections do show a strong correlation for the observed vs. calculated data as well as a strong comparison when comparing the raw field data to the data using the 2D inversion, proving a good fit for the inversion.

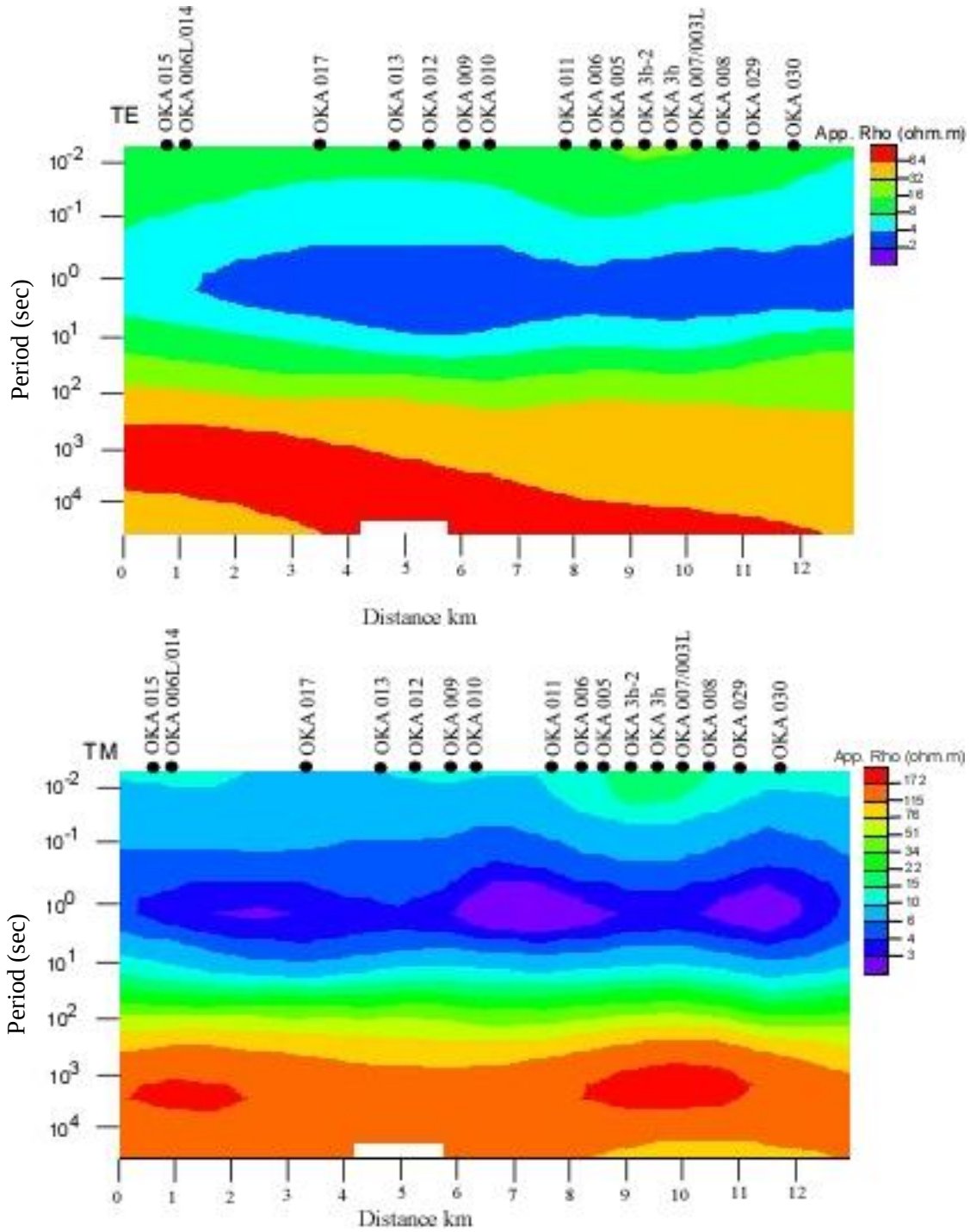


Figure 9. Pseudo-section using the raw data from field. The apparent resistivity is read for the TE (top) and the TM (bottom), both show three geoelectric layers.

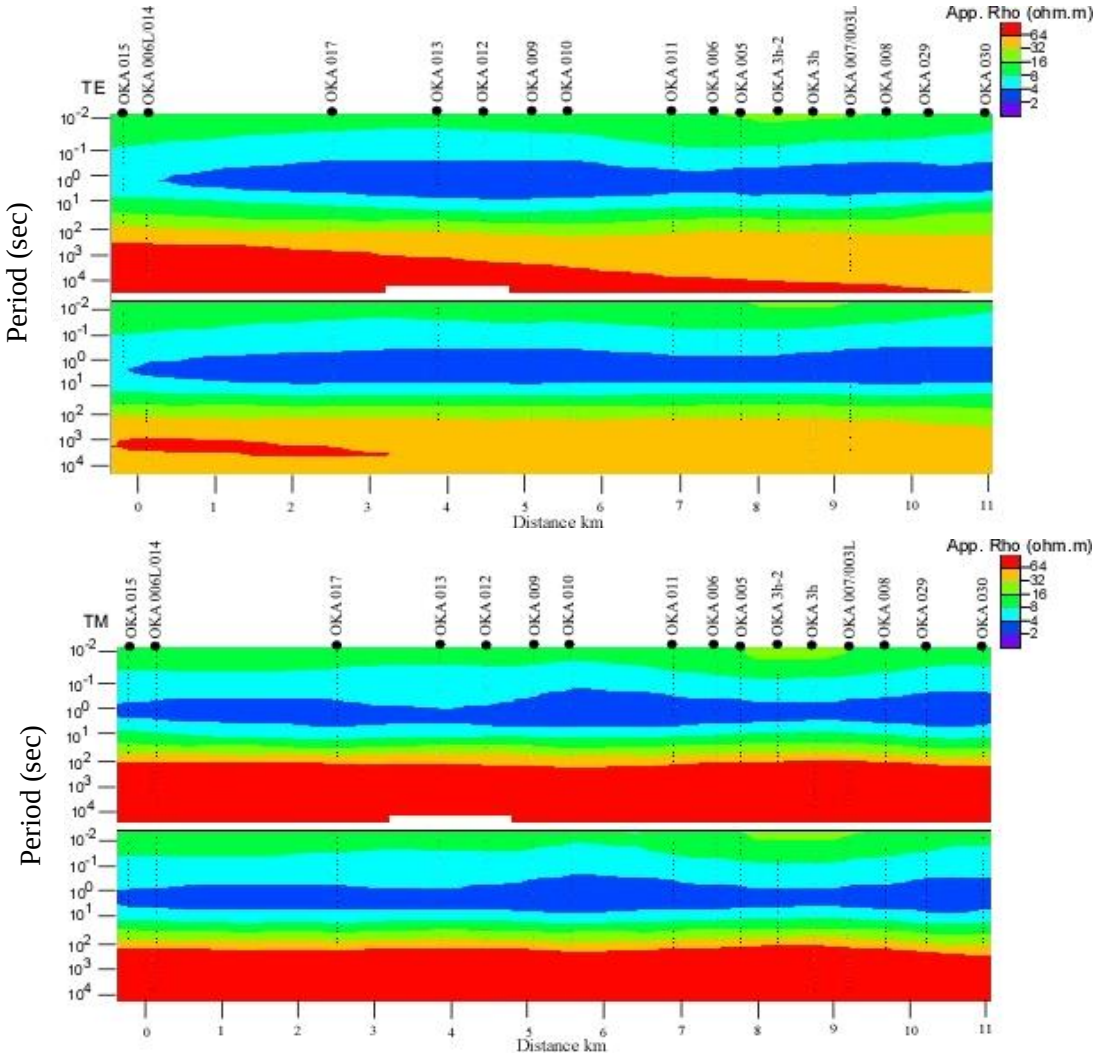


Figure 10. Pseud-section using 2D inversion model data with apparent resistivity. Warmer colors show higher resistivity and cooler are lower resistivity. For both the TE and TM sections, observed is plotted above the calculated apparent resistivity.

# CHAPTER IV

# RESULTS

## *4.1 Best Fit Lines and Inversion*

Utilizing the WingLink software, 400 iterations were run over the 18 MT stations used along the NE – SW profile. The final inversion had a root mean square (rms) error of 1.3947 and each of the individual station has rms error ranging from 0.72 – 1.96. The best-fit line for each station is shown in Figure 11. These represent the Transverse Electric (TE) and Transverse Magnetic (TM) sounding curves. On the graphs, the observed TE/TM is marked by dots, while the solid lines mark the calculated TE/TM values. The sounding curves show approximately two layers. One of the differences between the LEMI system, which are marked by an (L) at the end of the station name, and the Zen system is the periods. The LEMIs measure a narrower period (20-100 seconds) where the Zen systems measure a much broader band ($10^{-3}$ – $10^{3}$). This is easily seen in the sounding curve graphs where the LEMI have a much narrower curve.

These sounding curves only show the data that was used in the inversion; the cleaned points have been hidden and not used in the inversion. As shown, there are no outlying points on the sounding curves, which shows that the noise has been cleaned out. Although some of the rms error are slightly higher at 1.96, this was still < 2%, and the curves all showed a very smooth

line and matched with the calculated data. Also, as stated earlier, the removal of too much data will not provide enough to run the inversion with valuable results.

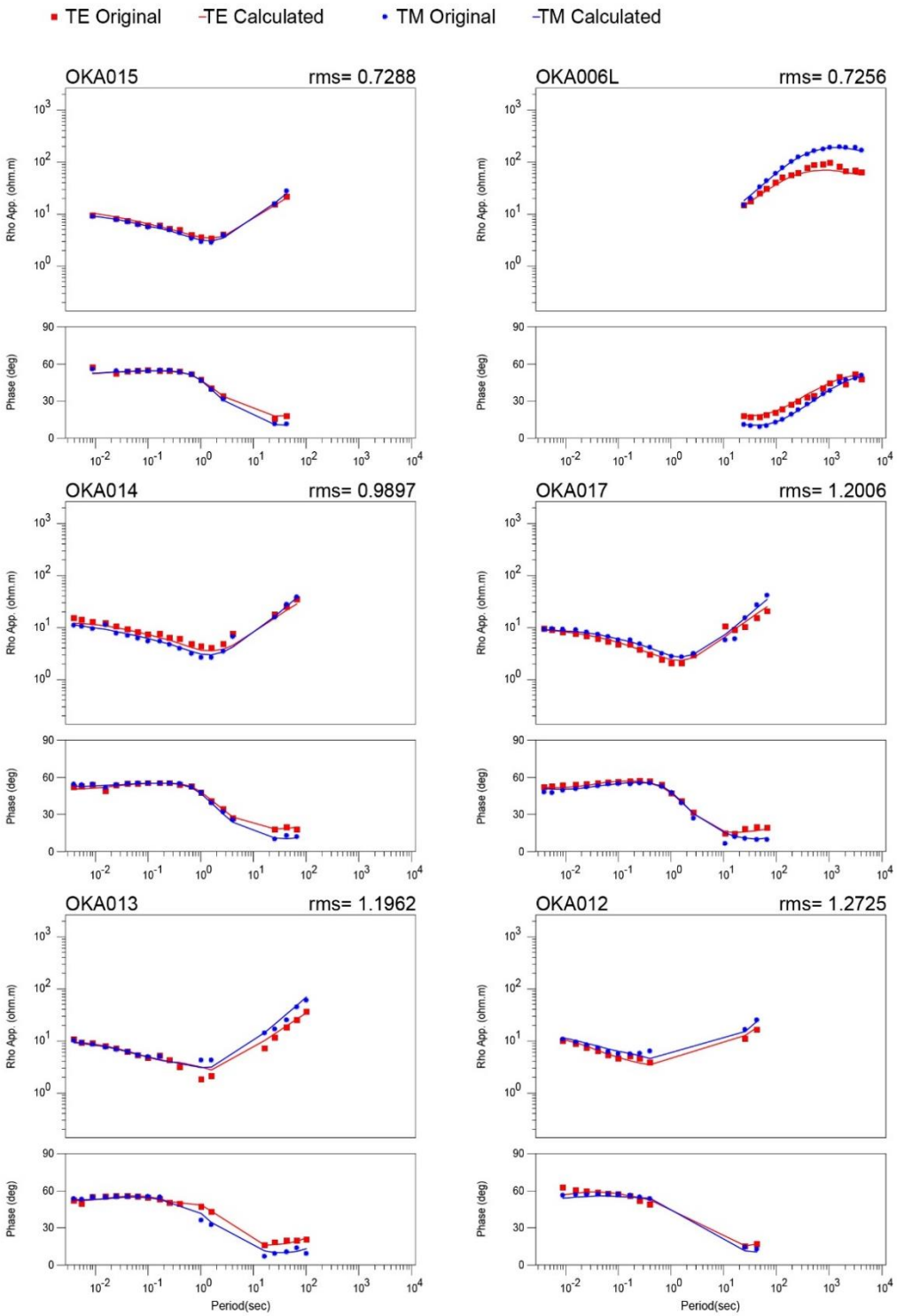

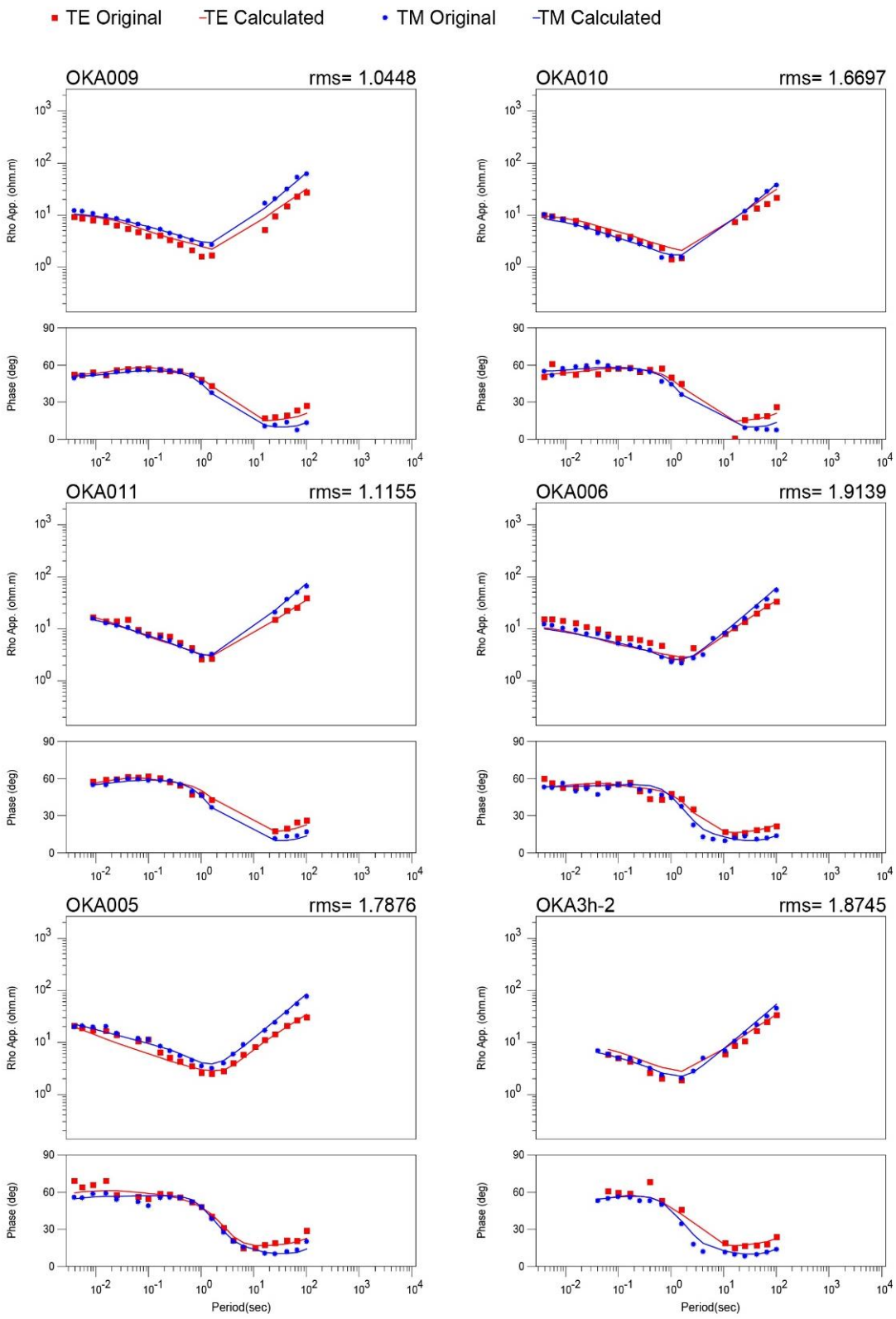
TE Original
TE Calculated
TM Original
TM Calculated
OKA009
rms= 1.0448
OKA010
rms= 1.6697
OKA011
rms= 1.1155
OKA006
rms= 1.9139
OKA005
rms= 1.7876
OKA3h-2
rms= 1.8745
Rho App. (ohm.m)
Phase (deg)
Period(sec)

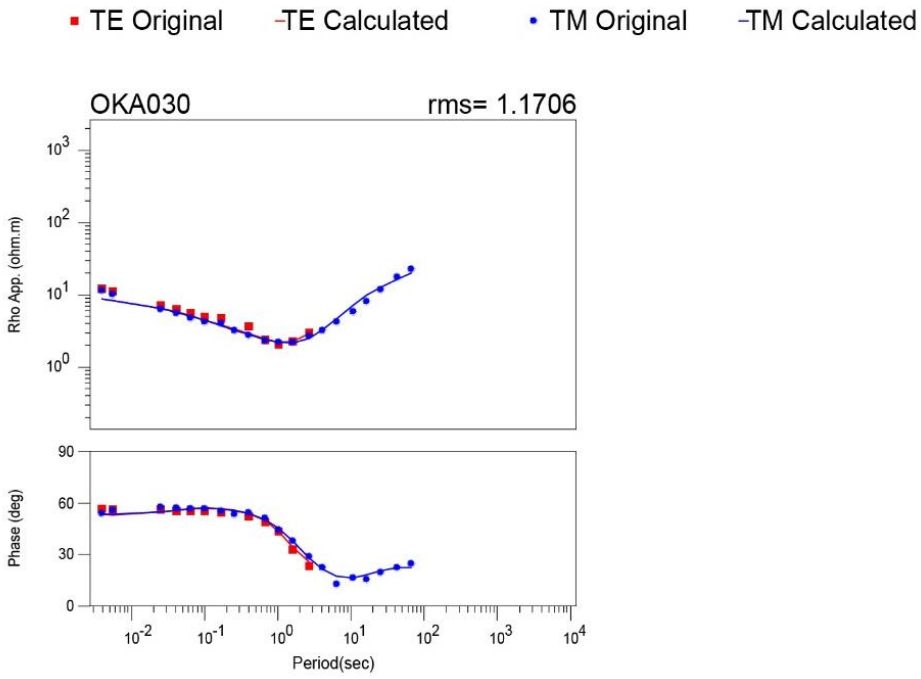


Figure 11. The best-fit line for TM and TE sounding curves of each station, which compares the calculated (solid line) against the original (dots) to see how the inversion fit the data. The root mean square (rms) error for each station is also displayed.

Figure 12 shows the stations locations along the NE-SW profile line along the WingLink inversion model. This smoothness constrained model has an RMS error of less than 2%, which indicates a good fit for the model done by the inversion and this is further shown when looking at the TE and TM sounding curves and comparing the observed against the calculated data (Figure 11). For this model, warm colors indicate low resistivity (high conductivity) and cooler colors indicate high resistivity (low conductivity). The inverted MT profile reveals two geoelectrical layers. The upper layer is from the surface to ~1.5 km and is composed of discontinuous, very high conductive lenses ranging from 1 to 43 ohm.m. These discontinuous lenses do not extend into the second layer except in two places. The second geoelectric layer is a highly resistive layer ($\geq$ 1000 ohm.m) and contains a conductive wedge from the surface to a depth of ~12 km where it reaches ~2-3 km in width and is defined by 12 to 285 ohm.m anomaly. Figure 13 is a schematic interpretation of the MT cross section illustrating the relationship of the sedimentary cover and the undulating Precambrian crystalline basement. Dashed lines on the schematic interpretation mark the two places where the discontinuous lenses penetrated the basement. The Sooner Lake Fault marked as a left-lateral strike slip fault is drawn in between MT stations OKA 005 and OKA 006 extending to depth. The high conductive anomaly wedge is contained in the red lines.

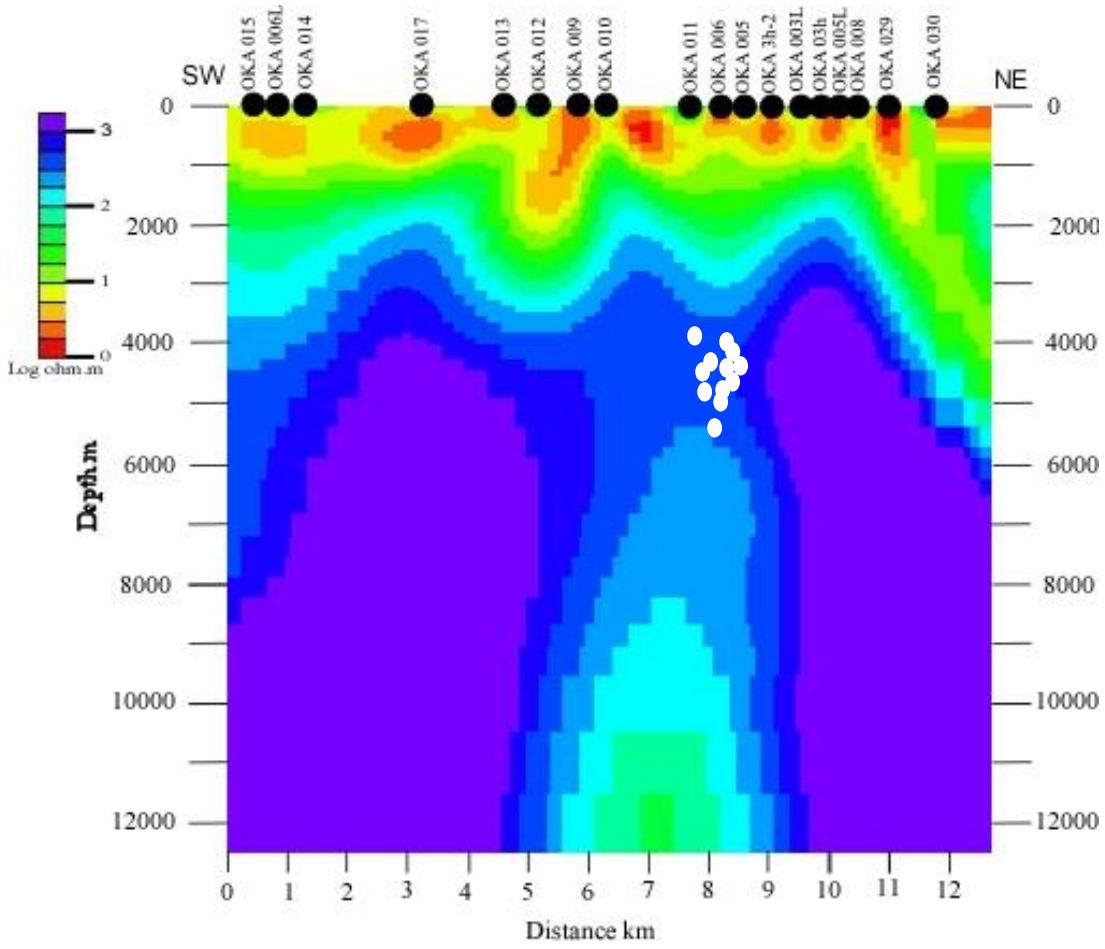


Figure 12. Two-dimensional (2D) isotropic resistivity inversion of the magnetotelluric (MT) data collected along the NE-SW profile. Warm colors represent more conductive (less resistive) domains while cold colors indicate less conductive (more resistive) domains. See Figure 7 for the location of the profile.

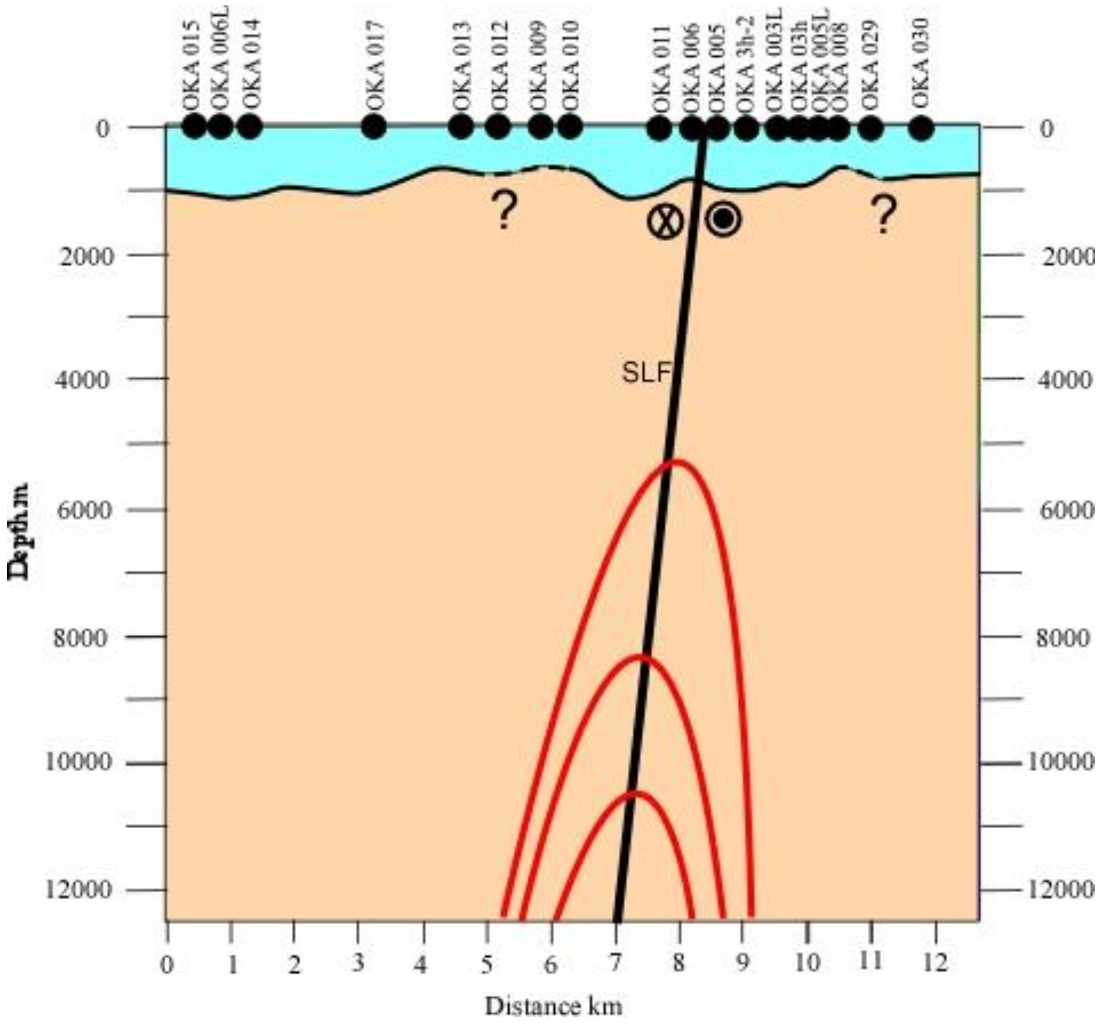


Figure 13. Schematic interpretation of the magnetotelluric (MT) inversion model showing the relationship between the sedimentary cover and the Precambrian crystalline basement, and the Sooner Lake Fault (labelled SLF) and the conductive anomaly wedge which is shown in red lines.

# CHAPTER V

# DISCUSSION AND CONCLUSIONS

## *5.1 Discussion*

The magnetotelluric (MT) inversions model (Figure 12) revealed details in geological features associated with the 2016 Pawnee, Oklahoma earthquake that have not been imaged by any other study. The upper geoelectric layer is defined by a series of discontinuous, highly conductive lenses (1-43 ohm.m) in the upper 1 km of the model. The stratigraphic cross-section in Figure 5 suggests that this geoelectric layer constitutes the sedimentary cover consisting of shales and limestone. The upper geoelectric layer overlays the lower geoelectric layer, interpreted to be the Precambrian crystalline basement, indicated by the cross-section in Figure 5. According to Archies Law, the bulk resistivity of a material is controlled by the porosity, saturation, and salinity. It is possible that the discontinuous lenses constituting the highly conductive upper geoelectric layer represent zones with the sedimentary cover that have highly saline fluids. By using Archies equation and a well in the area from Territory Resources named Oldham #8, bulk resistivity was found to be 1.1 ohm.m and porosity was found to be 24%, and a fluid resistivity was calculated to be 0.05 ohm.m, or a conductivity of 20,000 mS/m, which helps confirm the hypothesis that suggests very saline rich fluids in the upper 1 km. This helps explain the high conductive lenses shown in the inversion (Figure 12). Figure 13 shows that these lenses do

not extend into geoelectric layer 2 which constitutes the crystalline basement.

The basement is marked by high resistivity upwards of 1000 ohm.m. This data is supported by Becken et al. (2008) in their MT study of the San Andreas Fault in which very high resistivity values also marked the basement layer. In geoelectric layer 2, there is one zone that intrudes from geoelectric layer 1. This high conductive anomaly between stations OKA 005 and OKA 006 is interpreted to be the Sooner Lake Fault and is marked in the schematic cross-section in Figure 13.

When the earthquake data is overlain onto the inversion profile in Figure 12, the cluster of earthquakes coincides with the gap in conductivity along the fault and cluster between a 4-6 km depth. Since the profile does not directly intercept the mainshock area, nothing can be inferred about the conductivity of the seismogenic depth at the mainshock area where the injected fluids reactivated the fault. The aftershocks that spread through the location of the MT profile are secondary ruptures along the fault and may represent the propagation of the earthquake rupture front and therefore do not have a direct link to waste water injection. Only the southeastern segment of the Sooner Lake Fault hosted the majority of the aftershocks. This suggests that the rupture propagated southeastwards along the fault. The Sooner Lake Fault is defined by a steeply dipping ($80^{o}$ - $90^{o}$) and a wide (3-4.5 km) zone of increased conductivity relative to the surrounding basement blocks. We interpret this increased conductivity to reflect the presence of a wide zone of deformation along the fault. This zone of deformation is shown to extend > 10 km depth (refer to Figure 12). A study done by Heise et al. (2017) used a combination of MT and GPS to study the subduction interface along the Hikurangi Margin, New Zealand. They acquired MT across segments of the subduction zone and used GPS to map the actual movement of the fault blocks. The study found that the segments along the fault that showed movement from the GPS coincided with the MT data that showed high conductive zones and that the lower conductive zones from the MT study correlated to the blocks that showed no movement in the

GPS data. Heise et al. (2017) were able to show that the warmer, more conductive segments contained higher amounts of fluids, which in turn made those particular zones weaker and more likely to slip and move. This New Zealand study supports the interpretations that rupture zones are shown to be highly conductive when imaged using MT as well as a predominant factor in the Pawnee earthquake and the Sooner Lake Fault was waste water injection.

### *5.2 Conclusions*

This project was undertaken to provide some insight into the link between injected wastewater and the rupture processes. Due to the high conductivity of these metal rich and saline fluids, MT was decided as the best way to image these fluids in the Sooner Lake Fault Zone. Our results suggest an upper conductive sedimentary layer due to saline fluids. The Sooner Lake Fault is defined by a steeply dipping, wide (2-3 km) zone of increased conductivity relative to the surrounding resistive basement blocks. We interpret this increased conductivity to reflect the presence of a wide zone of deformation along the fault (i.e., wide zone of fracturing). This zone of deformation extends to >10 km depth and may have important implications for the Oklahoma faults that have hosted Mw > 5.0 earthquakes.

### *5.3 Future Work*

For the future work of this project, more MT lines are recommended over the main shock area better delineate the geometry of the Sooner Lake Fault and how it interconnects with the Labette Fault. Also, MT profiles need to be placed over the areas of the Labette and Watchorn Faults that did not rupture to see if there is any presence of fluids to gain more insight into why these specific parts did not rupture. It would be important to install MT equipment within the

study area for long term monitoring of fluid movement into the fault zones. This will provide more direct evidence linking fluid injection to seismicity.

Finally, the data acquired during this study can be obtained from the PIs (Drs Atekwana (atekwana@udel.edu), Key (kkey@ucsd.edu), and Evans (revans@whoi.edu)) and archived at the IRIS data repository https://www.iris.edu/hq.

# REFERENCES


Angerer, E., S. Crampin, T. L. Thomas, 2002, Processing, modeling and predicting time-lapse effects of overpressured fluid-injection in a fractured reservoir. Geophys. J. Int. 149, 267-280.

Becken, M., O. Ritter, S.K. Park, P.A. Bedrosian, U. Weckmann, M. Weber, 2008, A deep crustal fluid channel into the San Andreas Fault System near Parkfield, California, Geophysl. J. Int., 173, 718-732

Bedrosian, P., 2007, MT+, Integrating Magnetotellurics to Determine Earth Structure, Physical State, and Processes: Surveys in Geophysics, v. 28, p. 121-167.

Cagniard, L., 1953, Basic theory of the magneto-telluric method of geophysical prospecting: Geophysics, v. 18, p. 605-635.

Chen, X., N. Nakata, C. Pennington, J. Haffener, J.C. Chang, X. He, Z. Zhan, S. Ni, J.I. Walker, 2017, The Pawnee earthquake as a result of the interplay among injection, faults, and foreshocks, Scientific Reports, v. 7, doi: 10.1038/s41598-017-04992-z.

Denison, R.E. 1966, Basement rocks in adjoining parts of Oklahoma, Kansas, Missouri, and Arkansas, Ph.D. Dissertation, University of Texas, 291 pp., 1 plate.

Denison, R.E. 1981, Basement rocks in northeastern Oklahoma, Oklahoma Geological Survey Circular 84, 74 pp., 4 plates.

Denison, R.E., 1984, Geology and geochronology of Precambrian rocks in the Central Interior Region of the United States: Washington: U.S. G.P.O., Print.

Egbert, G.D., 1997, Robust multiple-station magnetotelluric data processing, Geophys. J. Int. 130, 475-496.

Fielding, E.J., S. Simran, D.P.S. Bekaert, V. Sergey, Samsonov, C.C. Jefferson, 2017, Surface Deformation of North-Central Oklahoma related to the 2016 Mw 5.8 Pawnee earthquake from SAR interferometry time series, SRL, vol. 88.

Grandin, R., M. Vallee, R. Lacassin, 2017, Rupture process of the Mw 5.7 Pawnee, Oklahoma, earthquake from Sentinel – 1 InSAR and seismological data, SRL, v. 88.

Harding, J.K., 2017, Mapping basement features associated with increased seismicity in central Oklahoma using aeromagnetic data, M.S. Thesis Oklahoma State University.

Healy, J.H., W.W. Ruby, D.T. Griggs, C.B. Raleigh, 1968, The Denver Earthquakes. Science 161.

Heise, W., T.G. Caldwell, S. Bannister, E.A. Bertrand, Y. Ogawa, S.L. Bennie, H. Ichihara, 2017, Mapping subduction interface coupling using magnetotellurics: Hikurangi margin, New Zealand, GRL, doi: 10.1785/0220170004.

Keranen, K.M., H.M. Savage, G.A Abers, E.S. Cochran, 2013, Potential induced earthquakes in Oklahoma, USA: Links between wastewater injection and the 2011 Mw 5.7 earthquake sequence, Geology, doi: 10/1130/G34045.1.

Langenbruch, C., and Zoback, M.D., 2016, How will induced seismicity in Oklahoma respond to decreased salt water injection rates?, Science Advances, V. 2.

McBee, w. (2003), The Nemaha and nearby fault zones in the context of Midcontinent strike-slip structural geology. Abstracts – AAPG Mid-Continent Section Meeting.

McNamara, D.E., G.P. Hayes, H.M Benz, R.A. Williams, N.D. McMahon, R.C. Aster, A. Holland, T. Sickbert, R. Hermann, R. Briggs, G. Smoczyk, E. Bergman, and P. Earle, 2015, Reactivated faulting near Cushing, Oklahoma: Increased potential for a triggered earthquake in an area of the United States strategic infrastructure, GRL. Lett. 42, 8328-8332 doi: 10.1002/2015GL064669.

Nolte, K.A., G.P. Tsoflias, T.S. Bidgoli, W.L. Watney, 2017, Shear-wave anisotropy reveals pore fluid pressure-induced seismicity in the U.S. midcontinent, Sci. Adv.

Northcutt, R.A., and Campbell, J.A., 1995, Geologic Provinces of Oklahoma, Oklahoma Geological Survey Open file Report OF 5-95, Map Scale: 1:750,000.

Pennington, C. and Chen, X., 2017, Coulomb stress interactions during the Mw 5.8 Pawnee Sequence, SRL v. 88.

Shah, A.K., and Keller, G.R., 2016, Geologic Influence on induced seismicity: constraints from potential field data in Oklahoma: GRL, v. 44, p. 152-161.

Vozoff, K., 1991, The magnetotelluric method, in Naibighian, M.N., ed., Electromagnetic methods in applied geophysics: Tulsa, Society of Exploration Geophysicists.

Yeck, W.L., G.P. Hayes, D.E. McNamara, J.L. Rubinstein, W.D. Barnhart, P.S. Earle, H.M. Benz, 2016, Oklahoma experiences largest earthquake during ongoing regional wastewater injection hazard mitigation efforts, GRL, v. 44, p. 711-717

VITA

DAVID JAMES BECKENDORFF

Candidate for the Degree of

Master of Science

Thesis: MAGNETOTELLURIC INVESTIGATION OF THE CAUSATIVE FAULT OF THE 2016 MW 5.8 PAWNEE, OKLAHOMA EARTHQUAKE

Major Field: Geology

Biographical:

Education:

Completed the requirements for the Master of Science in geology at Oklahoma State University, Stillwater, Oklahoma in May, 2018.

Completed the requirements for the Bachelor of Science in geology at Texas A&M University, College Station, Texas in 2016.

Experience:

Professional Memberships:
American Association of Petroleum Geologists (AAPG)
Oklahoma State University Geological Society (OSUGS)